Statistical properties of multi-directional waves propagating over a varying bathymetry

Jie Zhang[1,§], **Limin Huang**[1], **Michel Benoit**[2,3], **Yuxiang Ma**[4], **Saulo Mendes**[5]
[1]College of Shipbuilding Engineering, Harbin Engineering University, Harbin 150001, China
[2]EDF R&D, Laboratoire National d'Hydraulique et Environnement, Chatou 78400, France
[3]LHSV, ENPC, Institut Polytechnique de Paris, EDF R&D, Chatou 78400, France
[4]State Key Laboratory of Coastal and Offshore Engineering, Dalian University of Technology, Dalian, 116024, China
[5]School of Civil and Environmental Engineering, Nanyang Technological University, Singapore
[§]E-mail addresses: jie.zhang@hrbeu.edu.cn

1 INTRODUCTION

Recent studies have shown that strong and rapid depth variations can influence wave evolution over a long spatial extent, resulting in an enhanced occurrence probability of rogue waves downstream of the varying bathymetry [1, 2]. This occurs because the wave field is forced out of equilibrium by the non-equilibrium dynamics (NED) induced by the depth change, which continues to affect the wave field beyond the depth variation area until a new equilibrium state is eventually achieved. When NED governs wave evolution, both bound and free second-order harmonics are excited locally [3], and the intensified energy transfer among wave components results in a broadened spectrum when waves reach the new equilibrium state [4]. Moreover, evident non-Gaussian behaviour is observed in the high-order statistical moments of the free surface elevation (FSE) as well as in the wave crest and wave height distributions [5].

Research on NED under three-dimensional (3D) conditions has recently become a hotspot topic in this field. However, most studies rely on numerical simulations. Within the framework of the fully nonlinear potential flow model, the interplay between long-crested waves and two-dimensional bathymetry (circular shoals) has been investigated in [6] and [7], both identifying significant kurtosis enhancement atop the shoal due to NED. Using the high-order spectral method, Ducrozet and Gouin [8] found that directional wave spreading strongly suppresses rogue wave formation due to depth variation, while Tang *et al.* [9] reported a weaker directional effect. Conversely, Lyu *et al.* [10] showed, using a 2D depth-modified nonlinear Schrödinger equation, that short-crested wave fields with larger angular spreading may increase the occurrence probability of extreme waves. Remarkably, Mei *et al.* [11] found, through a fully nonlinear Boussinesq model, that directional spreading can decrease excess kurtosis in intermediate water depth but increase it in shallow water. Clearly, previous studies on NED of 3D waves have been either based purely on numerical simulations or constrained by experimental facility limitations [9]. These contradictory conclusions indicate that the effect of wave directionality on rogue wave formation remains unclear. To address this knowledge gap, we conduct a systematic, large-scale experimental study of NED in wave fields with varying directional spreading and incident angles.

2 EXPERIMENTAL TESTS

The experimental campaign was conducted at the Multi-functional Test Basin of the National Marine Environmental Monitoring Center (NMEMC) in Dalian, China. The wave tank is 49 m long, 47 m wide, and 1.2 m deep. Waves are generated by a snake-type (consisting of 80×0.5 m paddles) multi-directional wave maker installed on one shorter side of the tank. Porous media damping zones along the opposing end and lateral boundaries are set to minimize wave reflection.

In the wave tank, an isosceles trapezoidal prism parallel to the wavemaker was installed on an otherwise flat bottom. It consists of a central flat section (8 m in width and 0.36 m in height) flanked by two transitional slopes (with a horizontal extent of 1.75 m, thus a gradient of 1/4.86). The upslope of the trapezoidal prism starts 15 m away from the wavemaker. During the experimental campaign, the water depth near the wavemaker was set to $h_1 = 0.61$ m, thus $h_2 = 0.25$ m over the submerged structure. Twenty-six resistance-type wave gauges were deployed during the tests, with two arrays of five probes being used to estimate the directional spectra before and above the submerged bar. The sampling frequency of the probes is $f_s = 50$ Hz. The schematic of the experimental basin, as well as the locations of the wave gauges, are shown in Fig. 1.

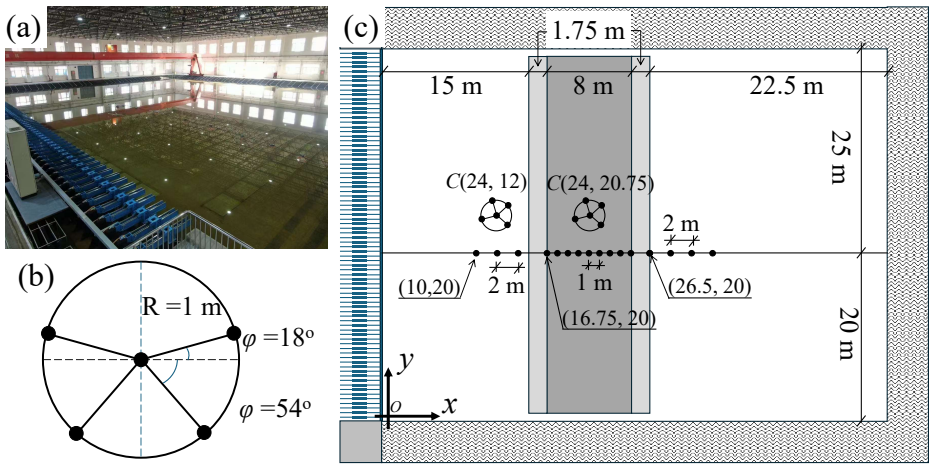

Figure 1: (a) NMEMC wave tank; (b) Layout of the wave gauge array for the estimation of directional spectrum; (c) Experimental wave tank and locations of the wave gauges.

The wave fields are described by their directional spectrum $S(f,\theta) = S_J(f)D(\theta|f)$, with $S_J(f)$ denoting the JONSWAP spectrum and $D(\theta|f)$ the classical Mitsuyasu-type directional spreading function. Since the formulations of $S_J(f)$ and $D(\theta|f)$ are well-known, they are not detailed here for the sake of conciseness. Here, the peak wave period $T_p = 1/f_p = 2.0$ s, and peakedness parameter $\gamma = 3.3$ are fixed. The dominant wave direction θ_{inc} and the directional spreading parameter $s_{\max}$ in the directional spreading function $D(\theta|f)$, are varied to examine the role of wave directionality on the NED effects. The configurations of incident wave fields are listed in table 1, together with non-dimensional parameters, wave steepness $\varepsilon \equiv \sqrt{2}k_p\sigma$ and relative water depth $\mu \equiv k_p h$, where σ denotes the standard deviation of the measured FSE and k_p the spectral peak wavenumber. The subscripts 0 and f denote deeper-water and shallower-water quantities, respectively. Three directional spreading conditions $s_{\max} = [10, 35, 85]$ were tested, corresponding to wide, intermediate and narrow directional

Case	$s_{\max}$	θ_{inc} [rad]	Deeper zone			Shallower zone		
			$H_{s,0}$ [m]	ε_0	μ_0	$H_{s,f}$ [m]	ε_f	μ_f
A	10	0	0.044	0.022	0.873	0.050	0.037	0.524
B	35	$[0, \pi/12, \pi/6, \pi/4]$	0.046	0.023		0.053	0.039	
C	85	0	0.046	0.023		0.054	0.040	
D	UNI	0	0.048	0.024		0.055	0.039	

Table 1: Incident wave conditions and key non-dimensional parameters

spreading, respectively. The case B series with $s_{\max} = 35$ was tested with one normal and three oblique incidence conditions, $\theta_{\text{inc}} = [0, \pi/12, \pi/6, \pi/4]$. Each experimental run lasts 6 minutes for wave generation and data acquisition, allowing for the limitation of energy accumulation due to long-wave reflection. To ensure statistical stability, several runs with different random phase seeds were performed such that the total sample duration exceeded $5{,}000T_p$ for each case.

3 RESULTS AND DISCUSSION

We focus on the evolution of statistical parameters characterizing departure from Gaussianity, namely skewness $\lambda_3(\eta) \equiv \langle(\eta - \langle\eta\rangle)^3\rangle/\sigma^3$ (with $\langle\cdot\rangle$ being an averaging operator) and kurtosis $\lambda_4(\eta) \equiv \langle(\eta - \langle\eta\rangle)^4\rangle/\sigma^4$ of the FSE. They both measure the magnitude of NED effects. We further use the net change of kurtosis $\Delta\lambda_4$ (with the offshore mean kurtosis subtracted) to measure the enhancement of rogue wave occurrence probability due to NED.

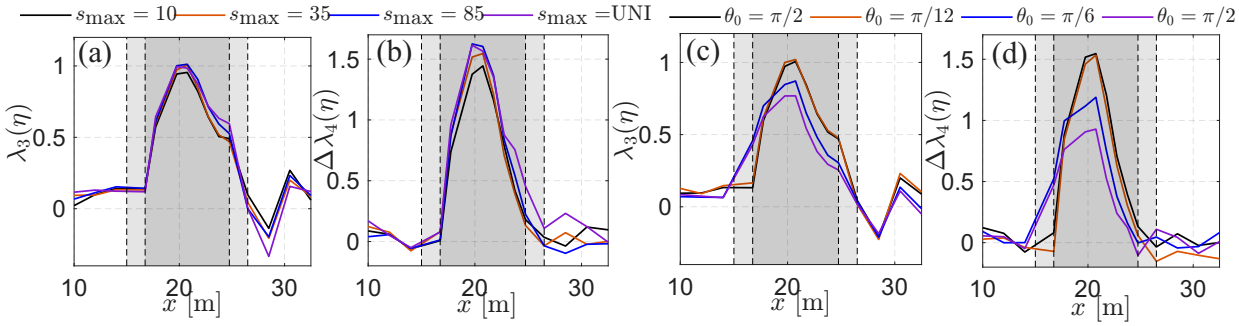

Figure 2: Spatial evolution of skewness and net change of kurtosis in the normal incident cases A–D in panels (a) and (b), and in the case B under oblique incident conditions in panels (c) and (d). The gray zone indicates the extent of the submerged bar, and the vertical dashed lines represent its edges.

Fig. 2 shows the spatial evolution of λ_3 and $\Delta\lambda_4$. In general, we see both are significantly enhanced over the bar, implying evident non-Gaussian characteristics due to NED. Waves are of vertically asymmetric shape on average, and higher rogue wave probability. From panels (a) and (b), we notice that skewness and net change of kurtosis are mildly reduced for broader directional spreading, λ_3 is very similar across all four cases, and for $\Delta\lambda_4$, the directional spreading makes only minor differences. In case D with $s_{\max} = \text{UNI}$ and $\theta_{\text{inc}} = 0$, the total kurtosis λ_4 maximum value achieves 4.61 over the bar, while in case A with $s_{\max} = 10$

and $\theta_{\text{inc}} = 0$, a comparable value, 4.44 is achieved. This observation is in line with the observations in [9], and in contrast to those in [10]. In Fig. 2(b) and (c), the effects of oblique incidence, which have been rarely discussed, are shown. We find that the incident angle plays an important role in the magnitude of the non-equilibrium wave response. This is attributed to the effective bottom slope: the larger the incident angle, the milder the effective slope gradient.

4 CONCLUSIONS

The present study provides a comprehensive experimental investigation into the effect of wave directionality on extreme wave formation during nonlinear shoaling, focusing on non-equilibrium dynamics induced by rapid depth changes. Our results indicate that directional spreading has a minor impact on reducing statistical moments such as skewness and kurtosis for a relatively steep slope, contrasting with previous numerical studies that suggest evident suppression of rogue wave formation due to energy dispersion with directionality. In contrast to the literature's limited exploration of oblique incidence, the present study highlights the significant role of the incidence direction in NED, driven by the effective bottom slope. This finding extends beyond previous works, which focused on normal incidence, by showing that obliqueness significantly reduces non-Gaussian behaviour and rogue wave formation.

REFERENCES

[1] Trulsen, K., Zeng, H., and Gramstad, O. 2012. Laboratory evidence of freak waves provoked by non-uniform bathymetry. *Phys. Fluids 24*, 097101.

[2] Zhang, J., Benoit, M., Kimmoun, O., Chabchoub, A., and Hsu, H.-C. 2019. Statistics of extreme waves in coastal waters: Large scale experiments and advanced numerical simulations. *Fluids 4*, 99.

[3] Li, Y., Draycott, S., Zheng, Y., Lin, Z., Adcock, T. A. A., and van den Bremer, T. S. 2021. Why rogue waves occur atop abrupt depth transitions. *J. Fluid Mech. 919*, R5.

[4] Zhang, J., Benoit, M., and Ma, Y. 2022. Equilibration process of out-of-equilibrium sea-states induced by strong depth variation: Evolution of coastal wave spectrum and representative parameters. *Coast. Eng. 174*, 104099.

[5] Mendes, S., Scotti, A., Brunetti, M., and Kasparian, J. 2022. Non-homogeneous analysis of rogue wave probability evolution over a shoal. *J. Fluid Mech. 939*, A25.

[6] Lawrence, C., Trulsen, K., and Gramstad, O. 2022. Extreme wave statistics of surface elevation and velocity field of gravity waves over a two-dimensional bathymetry. *J. Fluid Mech. 939*, A41.

[7] Draycott, S., and Li, Y. 2025. Extreme wave amplification through the interplay of wave nonlinearity and a two-dimensional bathymetry. *Phys. Fluids 37*, 026617.

[8] Ducrozet, G., and Gouin, M. 2017. Influence of varying bathymetry in rogue wave occurrence within unidirectional and directional sea-states. *J. Ocean Eng. Mar. Energy 3*, 309–324.

[9] Tang, T., Moss, C., Draycott, S., Bingham, H. B., van den Bremer, T. S., Li, Y., and Adcock, T. A. A. 2023. The influence of directional spreading on rogue waves triggered by abrupt depth transitions. *J. Fluid Mech. 972*, R2.

[10] Lyu, Z., Mori, N., and Kashima, H. 2023. Freak wave in a two-dimensional directional wavefield with bottom topography change. Part 1. Normal incidence wave. *J. Fluid Mech. 959*, A19.

[11] Mei, L., Chen, H., Yang, X., and Gui, F. 2023. Statistical properties of extreme waves in multidirectional wave fields over complex bathymetry. *Ocean Dyn. 73*, 827–849.